Electrical and thermal phenomena in low-density polyethylene/carbon black composites near the percolation threshold

Sohrab Azizi[1], Eric David[1], Michel F. Fréchette[2], Phuong Nguyen Tri [1, 3], Claudiane M. Ouellet-Plamondon[1,*]

[1] École de technologie supérieure (Université du Québec), 1100 Notre-Dame St W, Montreal, QC H3C 1K3 Canada

[2] Xi'an Jiaotong University, 28 Xianning W Rd, JiaoDa ShangYe JieQu, Beilin Qu, Xian Shi, Shaanxi Sheng, China

[3] Department of Chemistry, Montreal University, 2900, boul. Édouard-Montpetit, Montréal (Québec) H3T 1J4, QC, Canada

ABSTRACT

Low-density polyethylene (LDPE)/carbon black (CB) composites were fabricated via melt-compounding technique. The percolation threshold was found to be around 20 wt% CB, and an electrical network formed by conductive CB was proven by SEM investigation. Dielectric responses depicted an interfacial relaxation peak at 20 wt% CB content. LDPE/CB composites showed an electric field-dependent conductivity as well as a hysteresis behavior around the percolation threshold region. The CB particles with high thermal conductivity increased the heat conductance of the LDPE/CB20 up to 56%. The dynamic mechanical analysis (DMA) of the LDPE/CB composites exhibited a noticeable contribution of CB throughout the composites, increasing the storage and loss modulus. The physical interactions between CB particles in the

* Correspondence to: Claudiane M. Ouellet-Plamondon, Email address : Claudiane.Ouellet-Plamondon@etsmtl.ca

Department of Construction Engineering, École de technologie supérieure (ÉTS), Université du Québec, 1100 Notre-Dame St W, Montreal, QC H3C 1K3 Canada.

This is the peer reviewed version of the following article: Azizi, S., David, E., Fréchette, M. F., Nguyen-Tri, P. and Ouellet-Plamondon, C. M. (2019), Electrical and thermal phenomena in low-density polyethylene/carbon black composites near the percolation threshold. **Journal of Applied Polymer Science, 136**, 47043. doi: 10.1002/app.47043, which has been published in final form at https://doi.org/10.1002/app.47043.

filler network enhanced the thermal degradation of the LDPE/CB25 composite for more than 76 °C. The maximum breakdown strength of the LDPE/CB composites appeared with an approximately 10 % improvement for LDPE/CB5 than pure LDPE.

Keywords: composites, dielectric properties, thermal properties, extrusion, conducting polymers.

INTRODUCTION

Carbonaceous conductive particles have attracted a vast part of composite research due to a large number of potential industrial applications. A range of applications dealing with electromagnetic radiation shielding, self-regulating heaters,[1-3] high-voltage and high-temperature devices, high-performance EMI shielding materials,[4-6] and electrical field grading have been proposed for polyethylene/CB composites.[7] LDPE composites loaded with CB are attractive materials for electromagnetic interference (EMI) shielding applications thanks to their cost effectiveness, light weight, high resistance to corrosive conditions and easy processability.[4] These composites, at low filler concentration, can also be used for applications where the material remains insulating but in which electrical charges are allowed to slowly leak out of the material bulk in order to avoid space charge accumulation.[8,9] HVDC cables and spacecraft dielectrics are examples of such applications.[10,11] Therefore, possible applications for LDPE/CB composites cover the whole range of concentrations from low concentration for dielectric applications to intermediate concentration (near percolation threshold) for stress grading applications and up to high concentrations for EMI-shielding or semi-conductive screen applications.

Several studies have been conducted to investigate the electrical and thermal properties of LDPE/CB composites. Due to the role of finite and infinite CB clusters on the electrical conductivity of LDPE/CB composite, samples subjected to an electric field featured different behaviors. A non-ohmic trend at filler concentration close to the percolation threshold was observed due to the onset of current tunnels between CB clusters.[12] At the percolation threshold, a conducting pathway was formed resulting in a sharp increase of electrical conductivity. The application of a magnetic field on LDPE/CB nanocomposites prepared by thermoforming technique was found to increase the degree of crystallinity and reduce the electrical

conductivity.[13] The DC electrical conductivity of PE/CB nanocomposites was also found to decrease with the increase of temperature, particularly near the melting point.[14,15] These conductivity changes were linked to the positive temperature coefficient (PTC) factor of the composites, and affected by the filler concentration.[14-16] The multiwalled carbon nanotubes-core/thiophene polymer composite fabricated by chemical oxidative polymerization indicated a significant electrical and thermal conductivity enhancement as the results of π-π interaction between polymer and filler [17]. The compounded composite with carbon nanotube (CNTs) and polycaprolactam (PA6) illustrated a lower percolation threshold than the one with thermally reduced graphene oxide (TrGO). Furthermore, due to the presence of impurities within the TrGO, the electrical conductivity of TrGO composites was found to be lower than that of CNTs composites [18]. In the study done by Son et al., the thermally reduced graphene created an electrically conductive network throughout the polyester and poly(butylene terephthalate) (PBT) composite in which the electrical conductivity followed a power low at percolation threshold, leading to an increase of around 8 orders of magnitude with addition of ~ 0.2 -0.4 vol.% [19].

The thermal conductivity of polymeric composites containing high thermally conductive particles, such as carbon nanotubes and graphene as well as carbon particles, has been widely investigated. The thermal conductivity of composites has been related to many factors such as filler morphology and concentration, the strength of bonding between polymer and filler, the volume of side groups of the host matrix, defects, inherent thermal conductivity of filler and host polymer and processing conditions.[20,21] For example, the particle size of graphite in high-density polyethylene (HDPE) was found to play a predominant role on the thermal conductivity of the composite; graphite with diameter larger than 15 μm significantly intensified thermal conducting.[22]

According to these studies, several drawbacks such as poor miscibility and inappropriate filler dispersion have been reported for polyolefin-based/carbon-based composites. In this regard, additives play a predominant role. Thus, in comparison to different allotropes of carbon, CB provided a more uniform distribution, higher apparent density and faster flow rate during manipulation [23]. For this reason, the LDPE/CB remains an economical system that serves as a benchmark for polymer blends and nanoparticles. To the best of our knowledge, the hysteresis electrical effect and electrical field dependency of LDPE/CB composites as well as their thermal conductivity have been not so far reported. The aims of this study are to investigate the thermal conductivity of LDPE composite containing highly conductive CB and their dielectric response to different electric fields. In this regard, CB particle dispersion within the host matrix was investigated by scanning electron microscopy (SEM) and atomic force microscopy (AFM). Electrical field dependency, composite's memory behaviour subjected to the electrical field, and resistance of LDPE/CB composites at low CB content to high AC electrical fields were also examined. Thermal properties of the composites were assessed via differential scanning calorimetry and thermogravimetric analysis. Finally, dynamic mechanical properties of the composites were investigated.

EXPERIMENTAL

Materials

LDPE powder (XDS34P500) with a density of 0.922 $g.cm^{-3}$, a melt flow index of 0.4 $g.10\ min^{-1}$ and an average molecular weight of 102,000 was purchased from Marplex (Australia). Commercial CB particles (VXC500) possessing excellent electrical and thermal conductivity and low sulfur content was provided from Cabot, with an apparent density of 1.7-1.9 $g.cm^{-3}$ at 20 °C and an average particle size of 10 micrometers or less in diameter.

Sample preparation

The morphology of the composites was investigated by scanning electron microscopy (SEM) using Hitachi microscope (SU-8230 FE-SEM). The sample specimens were cryofractured by microtome in -100 °C liquid nitrogen and coated with a 2 nm platine using the turbo-pumped sputter (Q150T).

CB additive with different concentrations was blended with LDPE and the samples were labeled according to Table I. All samples were fabricated with a twin screw co-rotating extruder (Haake MiniLab II) at a 140 °C melting zone temperature and a 110 rpm screw rate. To obtain a better dispersion, the extruded compound was recycled through the internal bypass existing in the extruder. Each batch of the compound was extruded and recycled for 5 min. Polymer films with an average thickness of 0.3 mm were subsequently prepared by hot pressing at 155 °C and 6.5 MPa of loading pressure.

Table I.

Measurements

The composite morphologies were analyzed by atomic force microscopy (AFM) using a digital instrument multimode AFM (Veeco multimode) on a cross-section thin film prepared by cryogenic microtoming. These observations were carried out at room temperature and the data were acquired in the height, amplitude and phase modes with a scan rate of 1 Hz and areas of 4×4, 2×2 and 0.65 ×0.65 μm^2.

The dielectric response of LDPE/CB composites was measured using a flat disk with a diameter of 40 mm and an average thickness of 300 µm. The measurements were performed with a broadband dielectric spectrometer (Novocontrol) in a wide range of frequencies, ranging from

0.01 Hz to 1 MHz at 20 °C with an AC excitation voltage of 3 Vrms. The real part (ε'), the imaginary part (ε'') and the complex permittivity (ε^*) are given by Equation 1:[24]

$$\varepsilon^*(\omega) = \varepsilon'(\omega) - j\varepsilon''(\omega) \quad (1)$$

The AC breakdown strength (ACBD) of LDPE/CB composites at low filler contents was obtained with a Bauer DTA100 tester. These measurements were conducted according to the procedures described in the ASTM D149-09(2013) standard. A thin sheet was positioned between two ball-tip electrodes with a diameter of 4 mm and immersed into dielectric mineral oil. A short-term test consisting of 60 Hz voltage at a rising rate of 2 $kV.s^{-1}$ was employed for each measurement. The reported values were calculated from the average of ten trials in the same condition for each sample.

The resistance of the neat LDPE and LDPE/CB5 to erosion due to exposure to corona discharges was investigated by a handy-setup erosion tester. This type of test consisted of applying 10 kV rms at a frequency of 300 Hz for 35 h on a titanium ball with a diameter of 4 mm that was separated from a disk-shape sample with a diameter of 40 mm by a gap of 10 μm between the ball tip and sample surface. More information on this type of test and on the experimental setup can be found elsewhere.[25]

The structure of neat LDPE and its composite comprising CB filler was characterized using an X-ray diffractometer (PANanalytical X'Pert Pro). The scanning was conducted with Cobalt tube with Kα radiation (λ = 1.792 Å) in the range of 2ϴ from 15 to 65°. An accelerating voltage of 40 kV, a step size of 0.0668° and a counting time of 150 ms per step was applied.

The degree of crystallinity and melting temperature of LDPE/CB composites were obtained using differential scanning calorimetry (DSC) (Q20, TA Instruments). To remove the thermal

history of composites, the test specimen was first heated with a ramp of 10 °C.min^{-1} from 0 to 150 °C. It was cooled down from 150 to 0 °C with a rate of 10 °C.min^{-1}, and again, subsequently, the sample was heated similarly to the previous heating step. The DSC thermograms for the thermal properties assessment were obtained from the second heating cycle. The melting temperature as well as the specific fusion's enthalpy (ΔH_m) of the composites were extracted from the DSC thermograms, which allows the calculation of the degree of crystallinity (X_c) from Equation (2) [26]

$$X_c = \frac{\Delta H_m}{\Delta H_m^o} \frac{1}{(1-w)} \times 100 \quad (2)$$

where w is the filler content and ΔH_m^o (293.6 J.g^{-1}) is the specific fusion's enthalpy of perfect crystal of PE[27]. According to the variant of the Thomson-Gibbs equation for a lamellar crystallite of large lateral dimensions, the lamellar thickness (l) of pure LDPE and its composites is given by Equation 3, as follows:[28]

$$l = \frac{2\sigma_e}{\Delta H_m^0} \times \frac{T_m^o}{T_m^0 - T_m} \quad (3)$$

where, T_m^o is the thermodynamic melting point of infinite perfect crystals (418.6 K), T_m is the melting temperature, and σ_e is the fold-free surface energy (90.4 mJ.m^{-2}).[29]

Thermal stability of LDPE/CB composites as well as the content of CB in the samples were measured by thermogravimetric analysis (TGA) using a diamond TG/DTA instrument (Perkin Elmar). TGA experiments were carried out with samples around 10 to 13 mg in weight. The heating was performed with a ramp of 20 °C.min^{-1} from 200 to 800 °C under N_2 atmosphere and then the temperature was kept at 800 °C under air for 10 min.

The thermal conductivity of LDPE/CB composites was investigated using a guarded heat flow meter (DTC-25 TA instrument). Measurements were conducted according to the ASTM E1530-11(2016) standard, by applying a pressure of 20 psi from the upper surface on the sandwiched disk placed between two heating and cooling brass plates. The differential temperature between the heated and cooled brass plates was set to 25 °C. For each sample, the measurement was conducted on two replicates consisting of a circular disk with a diameter of 50.8 mm and a thickness of about 300 µm. In order to ensure the thermal stabilization of the sample chamber, the thermal conductivity measurement was performed after 2 h. The heat flowing across the sample was measured by a heat flux transducer which is located in the lower plate, and the thermal conductivity can then be inferred by Equation 4:[25]

$$\lambda = \frac{Q.t}{A.\Delta T} \qquad (4)$$

where Q represents the heat flux through the sample, A is the sample area, ΔT is the differential temperature between upper and lower plates and t is the sample thickness.

The dynamic mechanical properties of LDPE/CB composites were measured by a DMA Q800 (TA Instruments). Measurements were carried out in the tensile mode with a standard rectangular sample having dimensions of 30×7×0.3 mm^3 at a frequency of 1 Hz, deformation amplitude of 20 µm and a force track of 120 %. Each measurement was performed in a temperature range from -100 to 100 °C with a ramp of 5 $°C.min^{-1}$.

RESULTS AND DISCUSSION

SEM imaging

Figure 1 shows the cross-section morphology images of LDPE/CB composites at two magnifications. As indicated, the spheroid-shape CB particles throughout the LDPE/CB composites at below the percolation threshold (LDPE/CB15) were dispersed somehow uniformly, and the connections between particle-particle are not sufficient to form a conductive pathway (Figure 1a and 1b). The addition of more CB particles was found to form a connected network within the composite for LDPE/CB20 (at percolation threshold). At this filler content (LDPE/CB20) the chain-shape CB particles are seen clearly, leading bridges between the upper and lower electrode, and ease charge carrier (Figure 1c and 1d). At higher filler content (LDPE/CB25), a conductive network of the CB particles as well as several islands of the agglomerated CB particles were observed. Apparently, the CB particles acted as the nucleating agents in which caused some micron-sized filler agglomerations within the composite (Figure 1e and 1f).

Figure 1

AFM imaging

The cross-section cut surface morphology of LDPE/CB composites were observed by the AFM below (LDPE/CB15) and above (LDPE/CB25) the percolation threshold (Figure 2). The phase imaging in AFM showed rather uniform filler dispersion in the whole composite sample. The yellow and brown region in the phase images indicate the polymer matrix while the bright dots illustrate the CB particles. At filler concentrations below the percolation threshold (Figures 2a and 2b) some agglomerations were observed but overall, the CB particles were still mostly

isolated. Beyond the percolation threshold (LDPE/CB25), the CB particles were connected together, forming a conducting pathway in the polymer matrix (Figures 2c and 2d), and, as expected, a higher number of particle-to-particle connections were observed here than in the case of the composite containing 15 wt % CB. Further physically connected particles in the composite with high filler content (LDPE/CB25) will influence on electrical, mechanical and thermal properties of composites, as explained later.

Figure 2.

Dielectric properties

The frequency-domain dielectric response of LDPE/CB composites at 20 °C is shown in Figure 3 (real part, 3a and imaginary part, 3b). At low filler concentrations (under 20 wt%), a conductive network bridging both electrodes was not achieved[30], but at filler content around 20 wt%, while the DC conductivity remained very low, some conductive structures within the composite bulk started to form and gave rise to high dielectric losses featuring an interfacial loss peak in the vicinity of 1 Hz. This was in good agreement with SEM and AFM observations explained previously. This interfacial polarization mechanism in the composite led to a stepwise increase of the real permittivity part, as imposed by the Kramers-Kronig relations.[31,32] The interfacial relaxation mechanism, also known as Maxwell-Wagner-Sillars effect,[33] was a result of the accumulation of charge carriers at the interface of the slightly conductive clusters within the composites that were not yet bridging both electrodes'[3,34]. When the filler concentration reached the percolation threshold (CB contents between 20-25 wt %), the electrical conductivity of the composite switched from that of an insulating material to a semi-conductive one[35,36]. Thus, the conductivity of the LDPE/CB25 composite was found to increase by about 11 orders of magnitude compared to that of pure LDPE, as can be seen in Figure 4.

A comparative value of the electrical conductivity and the percolation threshold of several composites are presented in Table II. Composites prepared by solvent-casting were found to be conductive at extremely lower filler content than the melt compounding one. Due to the existence of some impurities such as oxygenated groups in the graphene-based fillers, composites with CB additive revealed higher electrical conductivity. In this regard, comparing our LDPE/CB composite with its counterparts indicate good electrical conductivity with respect to others referred composites.

Table 1I.

In order to better understand the origin and contribution of the charge carrier and charge accumulation in the interface of inclusions, the imaginary permittivity of the LDPE/CB20 composite at 20 °C was fitted according to Equation 5[32],

$$\varepsilon^*(\omega) = -i\left[\frac{\sigma_o}{\varepsilon_o \omega}\right]^N + \frac{\Delta\varepsilon}{(1+(i\omega\tau)^\alpha)^\beta} + \varepsilon_\infty \qquad (5)$$

where the first term represents the contribution from the charge carriers and the second term is the general empirical expression, the Havriliak-Negami function, used to model a relaxation process. σ_o and N are the material's parameters related to the conduction process, with N = 1 leading to the special case of direct conduction, $\Delta\varepsilon$ denotes the dielectric strength of the relaxation peak, τ is the relaxation time and the parameters α and β are the slopes of the low frequency side of the relaxation peak and the asymmetry parameter, respectively[32]. As can be seen in Figure 5, the use of Equation 5 gave a reasonable fitting of the relaxation peak of the LDPE/CB20 composite with a time constant of 6.2 x 10^{-2} s and a dielectric strength of 8.2. The parameters α and β are given in Table III as well as σ_o with N = 1 (direct conduction). At

higher frequencies than the peak frequency of the relaxation process, Equation 5 predicts a rapid decrease to essentially zero of the dielectric losses and consequently cannot fit any more the experimental data that exhibits an unusual constant-loss dielectric response. The complete fitting of the dielectric spectrum shown in Figure 5 can be achieved by the addition to Equation 5 of a third term, similar to the first one but with a low value of N in the vicinity of ~ 0.1.

Figure 3.

Figure 4.

Figure 5.

Table III.

Effect of temperature on the electrical responses

The electrical responses of the LDPE/CB composite at percolation threshold (LDPE/CB20) were investigated at different temperatures from 30 °C to approximately the polymer melting point (100 °C) (Figure 6). The findings showed a significant decrease of the dielectric losses with increasing temperature as well as a constant or "flat" dielectric loss behavior. This behavior, which has been known for decades for various solid materials, such as glasses and ferroelectric crystals[37], is still poorly understood. One possible reason for the decrease of dielectric losses with the increase of temperature might be the release of the absorbed moisture forming an interlayer between the hydrophilic particles and the hydrophobic matrix[38]. However, when the measurements were conducted for the second run at 40 and 30 °C consecutively after the elevated temperature (100 °C) run, the dielectric losses were found to increase again at approximately the same level as for the first run. Accordingly, the main contribution of the lowering of the dielectric losses was found to be linked to the thermal expansion of the composite for which the increase of

temperature (50 to 100 °C) causes a slight separation of previously connected particles[14,39-42]. When the dielectric response was measured for the second run (at 40 and 30 °C), due to the shrinkage of the composite, the electrical connectivity between closely located carbon particles increases, forming larger aggregates. As a result, both the real and imaginary parts of the complex permittivity of the LDPE/CB20 were found to increase significantly. Thus, the volume fraction of the CB particles (ϕ_{CB}) within the composite, as well as the microstructure, was affected by thermal expansion, which plays a remarkable role on the electrical properties of the composite[43-45]. The changes in the location of the interfacial relaxation peak with increasing temperature can be explained in a similar fashion by the disruption of the previously conductive aggregates (for 40, 50 and 60 °C). At higher temperatures up to 100 °C, the contribution of charge fluctuations throughout the composite bulk starts to be predominant at low frequency and leads to the usual low-frequency dispersion behavior.[46]

Figure 6

Non-linearity and hysteresis

Electrical field dependency of the dielectric response of pure LDPE and LDPE/CB composites was studied over the 10^{-1}-10^{-4} Hz frequency range. Measurements were conducted using different electrical fields, ranging from 17 to 1100 V.mm^{-1} (first run) and then lowering the electrical field to the initial value of the electrical field (second run). For LDPE/CB25 and LDPE/CB30 the measurements were carried out only at 17 and 178 V.mm^{-1}. The composites were found to exhibit significant electrical field dependency in their dielectric response in the vicinity of the percolation threshold, as illustrated in Figure 7a. In fact, the LDPE/CB20 composite featured a non-linear conductivity as well as a counterclockwise hysteresis behavior. Figure 7b illustrates the imaginary permittivity of LDPE/CB20 as a function of applied electric field. As can be observed,

a low frequency interfacial relaxation peak occurred at low electrical field during the first run but then moved towards higher frequencies as the field was increased. The peak disappeared when the field was further increased and the contribution of the DC conductivity started to dominate the low-frequency dielectric response. This shift of MWS peak towards higher frequencies is due to the increase of the intra-cluster connections leading to a more conductive cluster and consequently a lower relaxation time.[47] When the field reached values above 300 V.mm^{-1}, cluster-to-cluster connections started to appear and ultimately charge transportation through the material occurred.[48,49]

Figure 7.

AC breakdown

Dielectric AC breakdown strength was analyzed with the two-parameter Weibull distribution, and results are shown in Figure 8. According to this distribution, the failure probability under an increasing ramp of AC voltage is given by Equation 6:

$$P(E) = 1 - \exp\left[-\left(\frac{E}{\alpha}\right)^{\beta}\right] \quad (6)$$

where $P(E)$ represents the cumulative failure probability at an electrical field E, α is the scale parameter or the characteristic breakdown strength, which is the field for which 62.3 % of the samples have failed, and β is the shape parameter which is related to the scattering of the data obtained during the BD measurements[25]. A characteristic breakdown strength (α) of 117 kV.mm^{-1} was found for the LDPE/CB5 sample which was about 10 % higher than the one obtained for pure LDPE. This increase can be linked to the trapping of charge carriers, generated in the composite matrix at high electrical field[31,50]. Further additions of CB nanoparticles led to a

reduction of dielectric breakdown strength due to the formation of conductive clusters and consequently tunneling current between particles and clusters[51].

Figure 8.

Resistance to corona discharges

The eroded volume after exposure to corona discharges was subsequently evaluated by the use of a mechanical profilometer for the neat LDPE and two composite samples (LDPE/CB5 and LDPE/CB10). The erosion test was stopped after 10 h for LDPE/CB10 due to sample failure. Figure 9 shows the profiles of the eroded surfaces for LDPE and LDPE/CB5 after the erosion test was completed. As can be observed, the eroded areas were highly symmetrical around the tip of the HV titanium electrode. The resistance to corona discharges was evaluated based on the calculation of the eroded volume and it was found to decrease when 5 wt% CB was added to the LDPE polymer matrix. Indeed, the eroded volume, as measured by the profilometer, was found to be 3.05×10^9 μm^3 and 3.88×10^9 μm^3 for LDPE and LDPE/CB5, respectively, corresponding to a decrease of about 27 % in erosion resistance.

Figure 9.

Dispersion of CB in LDPE investigating by XRD

XRD experiment was carried out to evaluate the CB dispersion in LDPE polymers. As indicated in Figure 10, the XRD patterns did not feature any diffraction peaks derived from CB in the LDPE/CB composites, illustrating suitable dispersion of CB particles in the matrix. CB illustrated two broad reflections at 28.5° and 52°, revealing extremely lower crystallinity with respect to the observed sharp peak for the semicrystalline LDPE polymer at 24.3°.[52]. Additionally, due to high surface specific areas of the CB, restacking of the CB was occurred,

and resulted broad reflection peak. The broad peak at 28.5° corresponds to the (002) of the CB. Pure LDPE and its composites with CB indicated two peaks at 24.3° and 27.5° corresponding to (110) and (200) lattice planes. The appeared peaks were found to be fixed in their locations, indicating adequate exfoliation of polymer chains and poor particles agglomerations. [53]

Figure 10

Thermal properties

The incorporation of CB into the pure LDPE was not found to significantly alter the composite's melting point (T_m), indicating a broad melting range, commencing from ~ 40 °C (Figure 11). Furthermore, the addition of CB particles did not increase the degree of crystallinity (X_c), as the crystallinity percentage was found to remain almost constant with a negligible change within two percent with respect to the pure LDPE. The lamellar thickness (l) of the ordered regions was deduced from the melting temperature and calculated according to Equation 3. Similar values of lamellar thickness were found for pure LDPE and their composites, which again corroborates the fact that the incorporation of CB did not lead to significant change in the matrix morphology (Table IV). TGA measurements were conducted showing that pure LDPE started to undergo pyrolysis at about 375 °C and then undergoes a rapid decomposition down to basically no ash content.[54] The onset temperature ($T_{5\%}$), corresponding to 5 % of the sample weight loss, the $T_{50\%}$ corresponding to 50 % of the sample weight loss as well as the final remaining mass at 550 °C are given in Table IV for each composite. CB loading was found to increase the onset decomposition temperature, particularly in the case of the LDPE/CB25 sample. This enhancement of the thermal properties can be explained by possible weak physical interactions between particles[55,56] as well as the formation of a filler network within the composite. Decomposition temperature was also found to increase by the addition of CB, from

464 °C for the pure LDPE to about 500 °C and 492 °C for the LDPE/CB25 and LDPE/CB30 composites, respectively. This increase may due to the high thermal stability of CB itself[57] as well as the lower mobility of the polymer chains close to the additives[58,59]. The residual content at 550 °C was in good agreement with the nominal values, initially calculated during the formulation.

Figure 11

Table IV.

Thermal conductivity

Thermal conductivity measurements of LDPE/CB composites were in good agreement with what was found for the electrical conductivity, featuring a significant increase only for concentrations at or above the percolation threshold (Figure 12). Neat LDPE showed a thermal conductivity of 0.28 $W.m^{-1}K^{-1}$, which is mainly due to phonon transportation as the electronic contribution is negligible. The amorphous regions and free volumes in the LDPE scatter phonons, which reduces thermal transportation[60]. Since the DSC results did not show much change in the polymer morphology for the composites, it was expected that the thermal transportation done by the crystalline regions would also be predominant for the composite below percolation and would increase due to the contribution of the CB conductive network from the percolation point. In fact, the thermal conductivity of LDPE/CB composites at low filler content up to 15 wt% was found to slightly decrease (Figure 12), probably due to the thermal resistivity at interfacial layers between the particles and the host polymer and due to the additional scattering of the phonons.[33,61] Increasing CB content above 15 wt% was found to raise the thermal conductivity significantly as can be seen for the LDPE/CB20, LDPE/CB25 and LDPE/CB30 composites. The enhancement of

the thermal conductivity at high filler content was observed due to the dominant contribution to the thermal conductivity of electronic transport and phonons transportation through the network formed within the composite.

Figure 12.

Dynamic mechanical properties

The influence of CB inclusions on dynamic mechanical properties was investigated in terms of storage modulus (E'), loss modulus (E'') and damping factor (δ), and the results are shown in Figure 13. The storage modulus that expresses the stiffness of the composite, and the loss modulus that is related to the absorbed energy are shown as a function of temperature. Both properties were strongly temperature-dependent. The reduction of storage modulus with increasing temperature is related to the increase of the mobility of the amorphous regions within the semicrystalline composites.[62] Addition of CB to pure LDPE increased the storage modulus of composites. This can be attributed to the possible Van der Waals interactions between CB particles.[4] The loss modulus and damping factor (tan δ) (Figures 13b and 13c) showed two relaxation peaks over the temperature range from -100 to 100 ^{o}C. The first relaxation peak, around 60 °C (Figure 13c), is due to the fading of crystalline regions, and consequently the loss of the composite's mechanical strength. The second relaxation peak (Figure 13b) at about -25 °C, is related to the mobility of entire polymer chain motions in the amorphous regions.[63] The loss modulus of all LDPE/CB composites were higher than that of the pure LDPE, which might be because of the mesophases created between CB particles and polymer that causes the applied external energy by frictional forces between polymer and particles to dissapate.[63] The enhancement of the mechanical properties of composites with higher filler content with respect to

their counterparts with lower contents showed the contribution of the CB particles to the material's mechanical strength.[64,65].

Figure 13.

The comparison of the storage modulus of several polymeric composites compounded with carbonaceous fillers is reported in Table V. As indicated, different carbon-based fillers revealed different values of storage modulus at the same filler content. In comparison with the reported references, our CB/LDPE composite illustrated higher mechanical storage modulus than its counterparts; possibly to better dispersion, higher intrinsic mechanical properties of the filler or greater mechanical strength of the matrix.

Table V.

CONCLUSION

In summary, LDPE/CB composites compounded by means of melt compounding featured a sharp increase in electrical conductivity with the addition of 20 wt% or more of CB particles. SEM investigation and AFM phase imaging showed the formation of conducting pathways within the LDPE/CB composite at high filler concentration, while at low filler content, no connected pathways were observed. The storage modulus of LDPE/CB composites increased with the incorporation of CB within the polymer matrix. The composite thermal decomposition temperature increased considerably thanks to the high thermal stability of CB and formation of CB network in LDPE polymer. LDPE/CB composites showed electrical field dependency as well as hysteresis in their electrical properties at filler concentration around the percolation threshold. The dielectric breakdown strength was found to increase by around 10% with the addition of 5

wt% CB, which makes LDPE/CB composites a suitable material at low concentration for applications requiring insulation. The addition of CB to LDPE did not enhance the resistance of the composite to erosion due to corona exposure. LDPE/CB composites with electrical conductivity of about 10^{-4} S/m (above the percolation) are suitable materials for semiconductive applications, having appropriate mechanical and thermal properties.

Acknowledgment

The Natural Sciences and Engineering Research Council of Canada is acknowledged to support this study.

References

1. Feller, J. F.; Bruzaud, S.; Grohens, Y. *Materials Letters.* **2004**, 58, 739.

2. Villacorta, B. S.; Ogale, A. A.; Hubing, T. H. *Polymer Engineering & Science.* **2013**, 53, 417.

3. Yuan, Q.; Wu, D. *Journal of applied polymer science.* **2010**, 115, 3527.

4. Mondal, S.; Ganguly, S.; Rahaman, M.; Aldalbahi, A.; Chaki, T. K.; Khastgir, D.; Das, N. C. *Physical Chemistry Chemical Physics.* **2016**, 18, 24591.

5. Villacorta, B. S.; Ogale, A. A. *Journal of Applied Polymer Science.* **2014**, 131.

6. Nisar, M.; Bergmann, C. P.; Geshev, J.; Quijada, R.; Maraschin, T.; de Souza Basso, N. R.; Barrera, E. G.; Galland, G. B. *Journal of Applied Polymer Science.* **2017**, 134.

7. Foulger, S. H. *Journal of Polymer Science Part B: Polymer Physics.* **1999**, 37, 1899.

8. Li, B.; Xu, X. B.; Li, Z. M.; Song, Y. C. *Journal of applied polymer science.* **2008**, 110, 3073.

9. Azizi, S.; Ouellet-Plamondon, C.; David, E.; Fréchette, M. Electrical Insulation and Dielectric Phenomenon (CEIDP), 2017 IEEE Conference on, 2017, pp 517. 2017.

10. Mazzanti, G.; Marzinotto, M., Extruded cables for high-voltage direct-current transmission: advances in research and development; John Wiley & Sons: **2013**.

11. Ryden, K. A.; Hands, A. D. *IEEE Transactions on Plasma Science.* **2017**, 45, 1927.

12. Nakamura, S.; Sawa, G. *1998 International Symposium on Electrical Insulating Materials, Proceedings.* **1998**, 333.

13. Ma, F. L.; Han, B. Z.; Wang, Y. J.; Jiang, H. *Icpadm 2009: Proceedings of the 9th International Conference on Properties and Applications of Dielectric Materials, Vols 1-3.* **2009**, 1192.

14. Hindermann-Bischoff, M.; Ehrburger-Dolle, F. *Carbon.* **2001**, 39, 375.

15. Tang, H.; Chen, X.; Luo, Y. *European polymer journal.* **1997**, 33, 1383.

16. Di, W.; Zhang, G.; Xu, J.; Peng, Y.; Wang, X.; Xie, Z. *Journal of Polymer Science Part B: Polymer Physics.* **2003**, 41, 3094.

17. Reddy, K. R.; Jeong, H. M.; Lee, Y.; Raghu, A. V. *Journal of Polymer Science Part A: Polymer Chemistry.* **2010**, 48, 1477.

18. Méndez, R.; Constant, B.; Garzon, C.; Nisar, M.; Nachtigall, S. M. B.; Quijada, R. *Polymer.* **2017**, 130, 10.

19. Son, D. R.; Raghu, A. V.; Reddy, K. R.; Jeong, H. M. *Journal of Macromolecular Science, Part B.* **2016**, 55, 1099.

20. Han, Z.; Fina, A. *Progress in polymer science.* **2011**, 36, 914.

21. Kochetov, R.; Andritsch, T.; Morshuis, P. H. F.; Smit, J. J. *Ieee Transactions on Dielectrics and Electrical Insulation.* **2012**, 19, 107.

22. Ye, C. M.; Shentu, B. Q.; Weng, Z. X. *Journal of Applied Polymer Science.* **2006**, 101, 3806.

23. Chen, B.-Y.; Hwang, K.-S. *Powder Metallurgy.* **2010**, 53, 51.

24. Håkansson, E.; Amiet, A.; Nahavandi, S.; Kaynak, A. *European polymer journal.* **2007**, 43, 205.

25. Heid, T.; Fréchette, M.; David, E. *IEEE Transactions on Dielectrics and Electrical Insulation.* **2015**, 22, 1176.

26. Suñer, S.; Joffe, R.; Tipper, J.; Emami, N. *Composites Part B: Engineering.* **2015**, 78, 185.

27. Ratanakamnuan, U.; Aht-Ong, D. *Journal of applied polymer science.* **2006**, 100, 2717.

28. Psarski, M.; Piorkowska, E.; Galeski, A. *Macromolecules.* **2000**, 33, 916.

29. Furushima, Y.; Nakada, M.; Murakami, M.; Yamane, T.; Toda, A.; Schick, C. *Macromolecules.* **2015**, 48, 8831.

30. Zhou, S.; Hrymak, A.; Kamal, M. *Journal of Applied Polymer Science.* **2017**, 134.

31. Dang, Z.-M.; Yuan, J.-K.; Zha, J.-W.; Zhou, T.; Li, S.-T.; Hu, G.-H. *Progress in Materials Science.* **2012**, 57, 660.

32. Kremer, F.; Huwe, A.; Schönhals, A.; Rózanski, S., 6 Molecular Dynamics in Confining Space; Springer: **2012**.

33. Burger, N.; Laachachi, A.; Ferriol, M.; Lutz, M.; Toniazzo, V.; Ruch, D. *Progress in Polymer Science.* **2016**, 61, 1.

34. Yu, J.; Zhang, L.; Rogunova, M.; Summers, J.; Hiltner, A.; Baer, E. *Journal of applied polymer science.* **2005**, 98, 1799.

35. Mysiukiewicz, O.; Sterzyński, T.; Ławniczak, P.; Rogodzińska, M. *Journal of Applied Polymer Science.* **2017**, 134.

36. Ren, D.; Zheng, S.; Wu, F.; Yang, W.; Liu, Z.; Yang, M. *Journal of Applied Polymer Science.* **2014**, 131.

37. Jonscher, A. K., Universal relaxation law: a sequel to Dielectric relaxation in solids; Chelsea Dielectrics Press: **1996**.

38. David, E.; Fréchette, M. *IEEE Electrical Insulation Magazine.* **2013**, 29, 29.

39. Yacubowicz, J.; Narkis, M. *Polymer Engineering & Science.* **1986**, 26, 1568.

40. Shen, L.; Wang, F.; Yang, H.; Meng, Q. *Polymer testing.* **2011**, 30, 442.

41. Zhang, P.; Wang, B. b. *Journal of Applied Polymer Science.* **2018**, 46453.

42. Traina, M.; Pegoretti, A.; Penati, A. *Journal of applied polymer science.* **2007**, 106, 2065.

43. Bueche, F. *Journal of Applied Physics.* **1973**, 44, 532.

44. Webb, A. J.; Bloor, D.; Szablewski, M.; Atkinson, D. *ACS Appl Mater Interfaces.* **2014**, 6, 12573.

45. Dudić, D.; Škipina, B.; Dojčilović, J.; Novaković, L.; Kostoski, D. *Journal of Applied Polymer Science.* **2011**, 121, 138.

46. Helal, E.; Pottier, C.; David, E.; Fréchette, M.; Demarquette, N. *European Polymer Journal.* **2018**.

47. Song, Y.; Zheng, Q.; Yi, X. S. *Journal of Polymer Science Part B: Polymer Physics.* **2004**, 42, 1212.

48. He, L. X.; Tjong, S. C. *Synthetic Metals.* **2011**, 161, 540.

49. Donzel, L.; Greuter, F.; Christen, T. *IEEE Electrical Insulation Magazine.* **2011**, 27.

50. Helal, E.; Demarquette, N. R.; David, E.; Fréchette, M. IEEE Electrical Insulation Conference (EIC), 2016, 2016, pp 592.

51. Tian, F.; Lei, Q.; Wang, X.; Wang, Y. *IEEE Transactions on Dielectrics and Electrical Insulation.* **2012**, 19.

52. Hu, E.; Hu, X.; Liu, T.; Liu, Y.; Song, R.; Chen, Y. *Applied Surface Science.* **2013**, 270, 596.

53. Lei, H.; Liu, Z.; He, C.; Zhang, S.-C.; Liu, Y.-Q.; Hua, C.-J.; Li, X.-M.; Li, F.; Chen, C.-M.; Cai, R. *RSC Advances.* **2016**, 6, 101492.

54. Ruvolo Filho, A.; Menezes, A. J. d.; Scarpa, P. S. d. N. *Materials Research.* **2008**, 11, 175.

55. Kuilla, T.; Bhadra, S.; Yao, D.; Kim, N. H.; Bose, S.; Lee, J. H. *Progress in polymer science.* **2010**, 35, 1350.

56. Huang, C. L.; Chen, Y. C.; Wang, C.; Tu, C. F.; Liao, F. S. *Journal of Applied Polymer Science.* **2013**, 130, 1038.

57. Crompton, T. R., Thermal Stability of Polymers; Smithers Rapra: **2012**.

58. Gabbott, P., Principles and applications of thermal analysis; John Wiley & Sons: **2008**.

59. Yang, S.; Taha-Tijerina, J.; Serrato-Diaz, V.; Hernandez, K.; Lozano, K. *Composites Part B: Engineering.* **2007**, 38, 228.

60. Huang, X.; Jiang, P.; Tanaka, T. *IEEE Electrical Insulation Magazine.* **2011**, 27.

61. Ghose, S.; Watson, K. A.; Working, D. C.; Connell, J. W.; Smith, J. G.; Sun, Y. P. *Composites Science and Technology.* **2008**, 68, 1843.

62. Menard, K. P., Dynamic mechanical analysis: a practical introduction; CRC press: **2008**.

63. Huang, Y.; Jiang, S.; Wu, L.; Hua, Y. *Polymer Testing.* **2004**, 23, 9.

64. Fathi, A.; Hatami, K.; Grady, B. P. *Polymer Engineering & Science.* **2012**, 52, 549.

65. Wu, G.; Zheng, Q.; Zhang, M.; Hou, Y. *Journal of applied polymer science.* **2006**, 100, 4127.

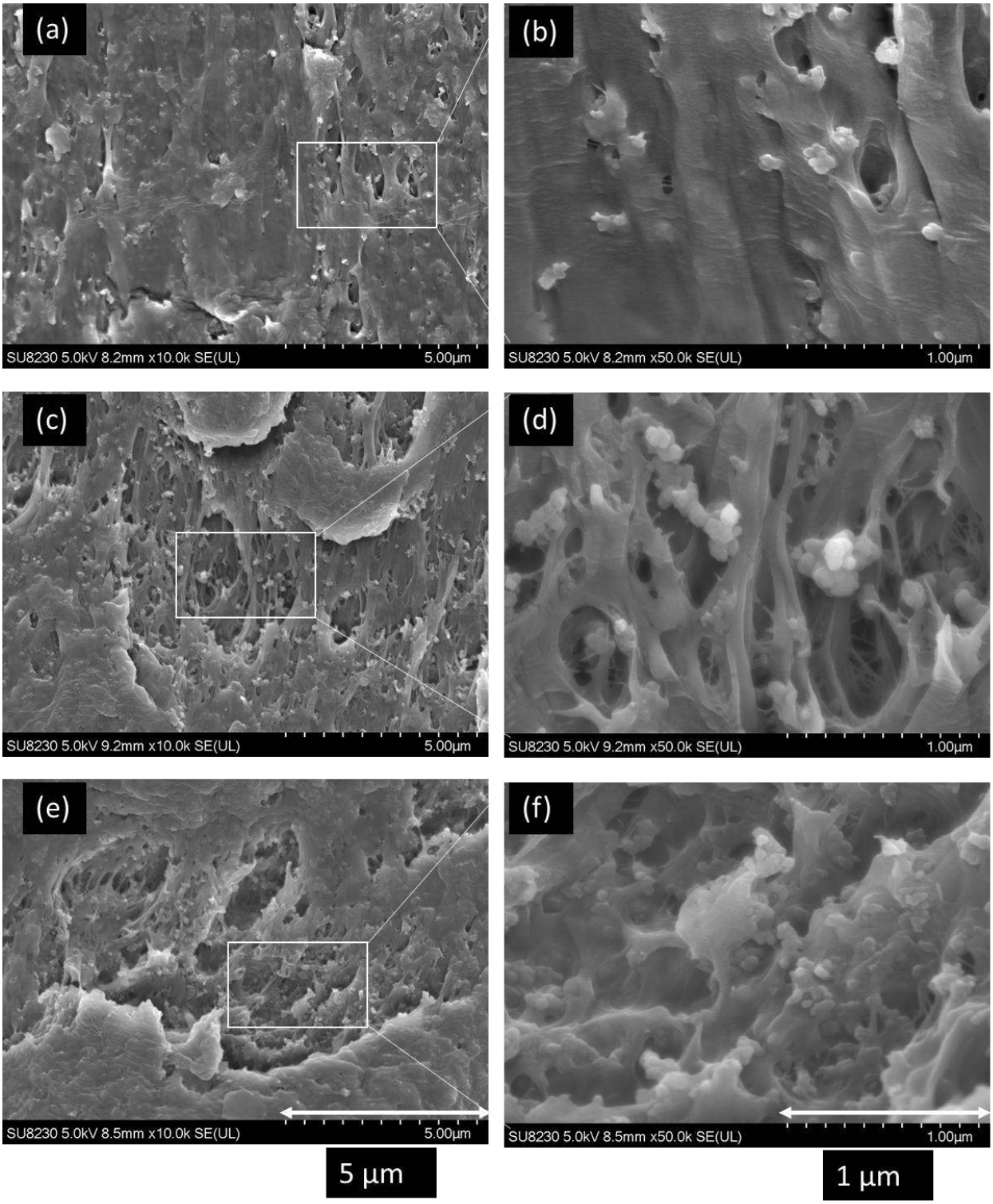

Figure 1. SEM images of the cross-sectioning cut of the LDPE/CB composites: (a, b) LDPE/CB15, (c, d) LDPE/CB20 and (e, f) LDPE/CB25 at 10k and 50k magnifications, respectively.

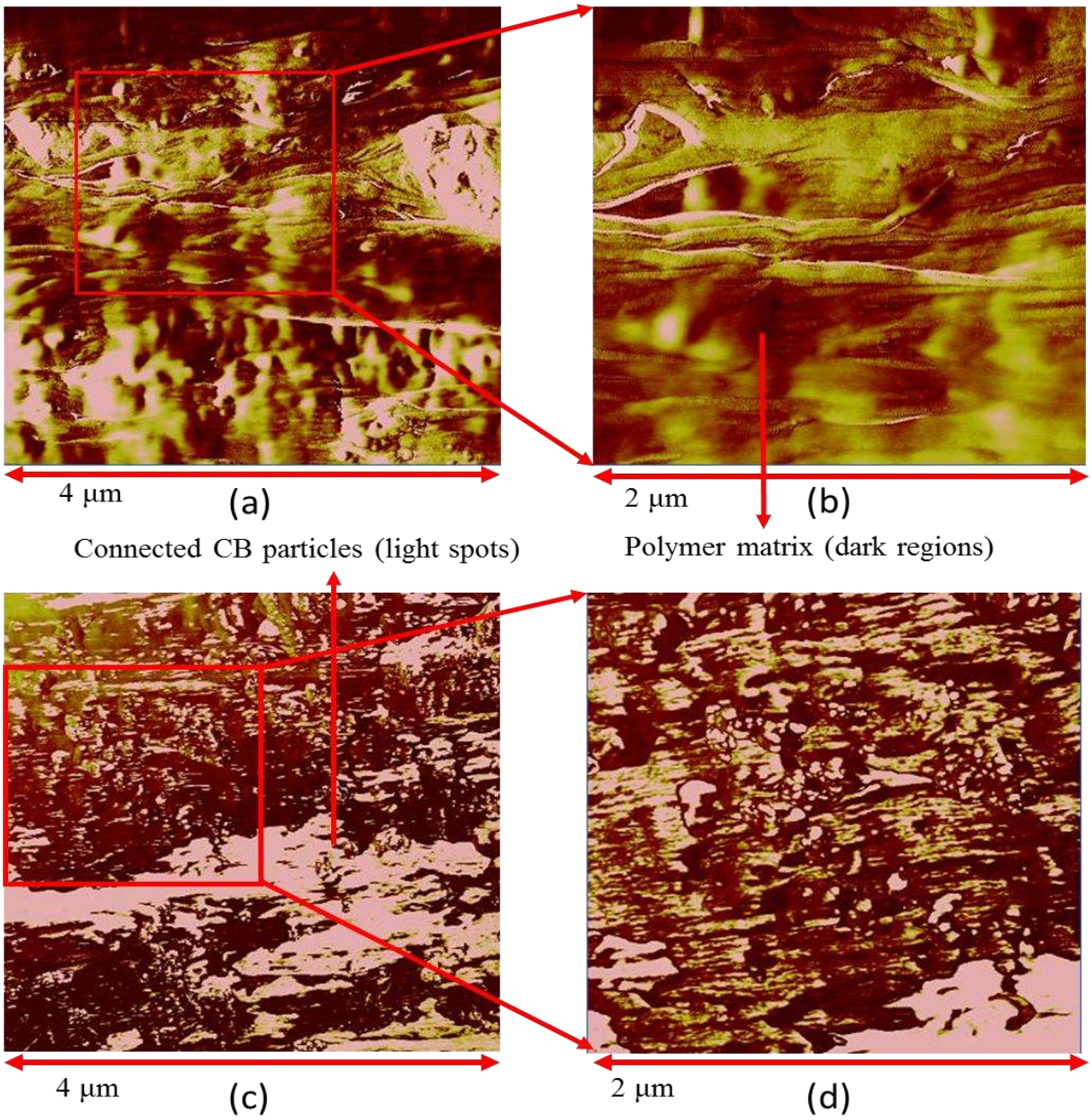

Figure 2. AFM phase images at different magnifications: (a, b) LDPE/CB15, (c, d) LDPE/CB25.

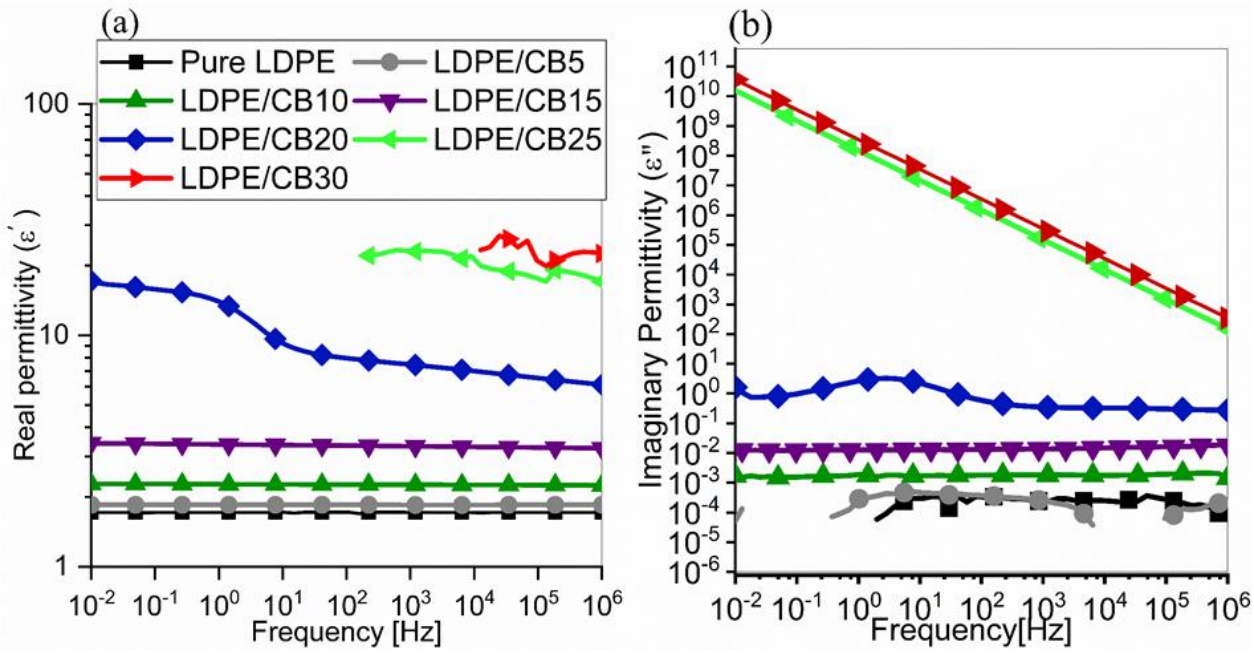

Figure 3. Real (a) and imaginary permittivity (b) of LDPE/CB composites at 20 °C as a function of frequency.

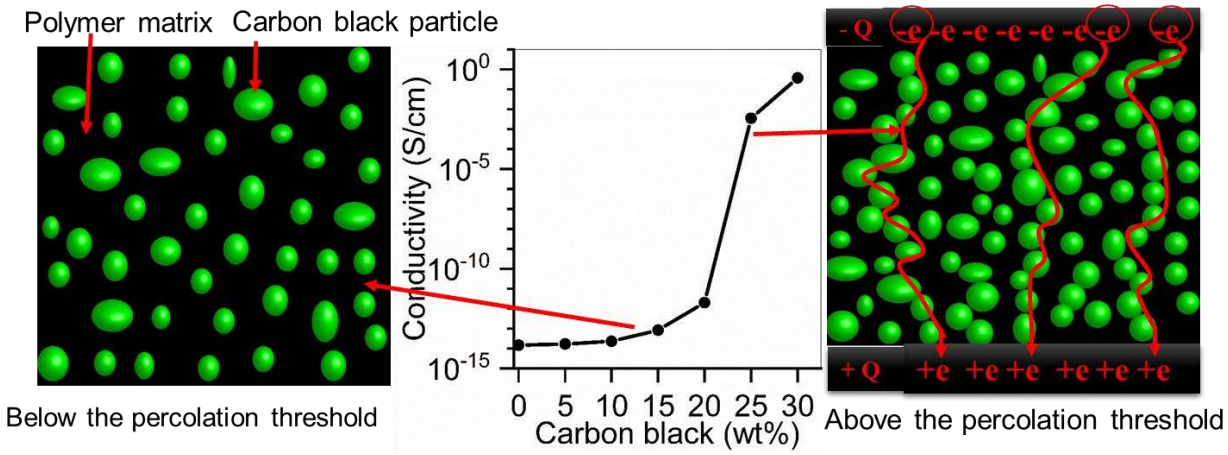

Figure 4. Charge carrier diagram and electrical conductivity of LDPE/CB composite as a function of CB concentration.

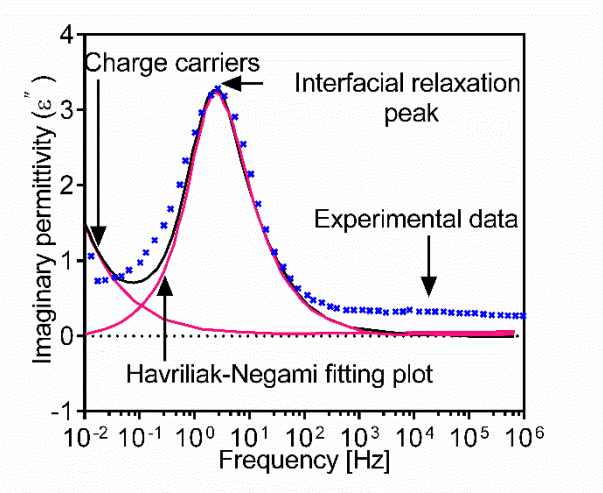

Figure 5. Imaginary permittivity of LDPE/CB20 as a function of frequency at 20 °C, fitted with Equation (5), the black curve representing the sum of the contribution from the DC conductivity and the interfacial relaxation process.

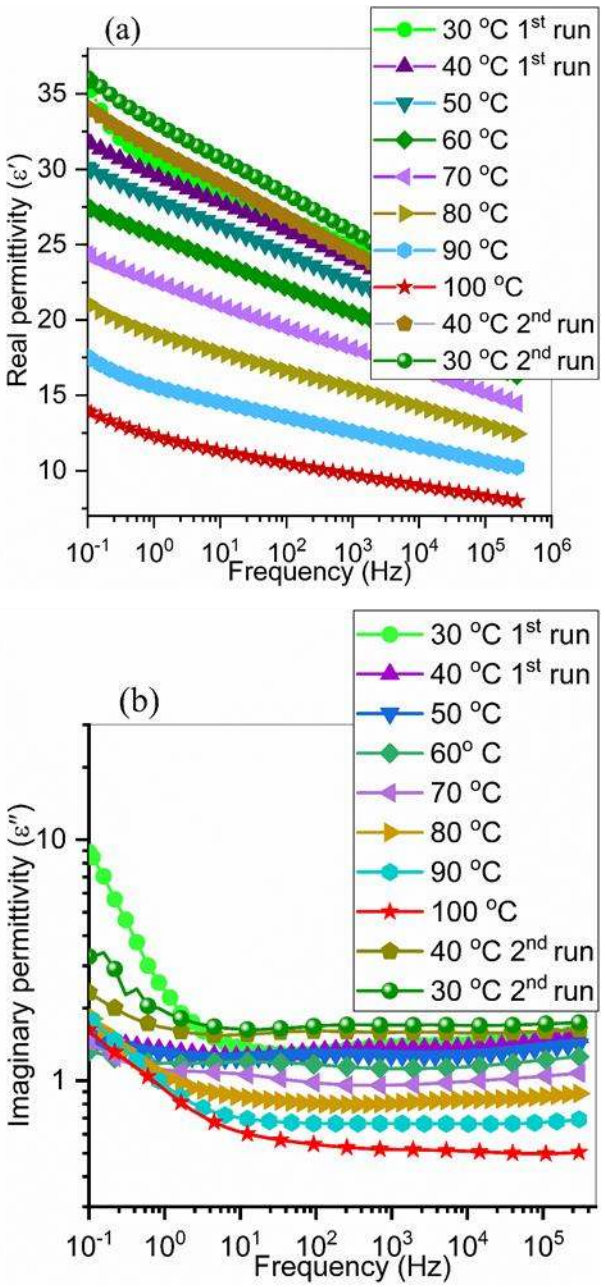

Figure 6. Real and imaginary parts of the complex permittivity of LDPE/CB20 as a function of frequency at various temperatures.

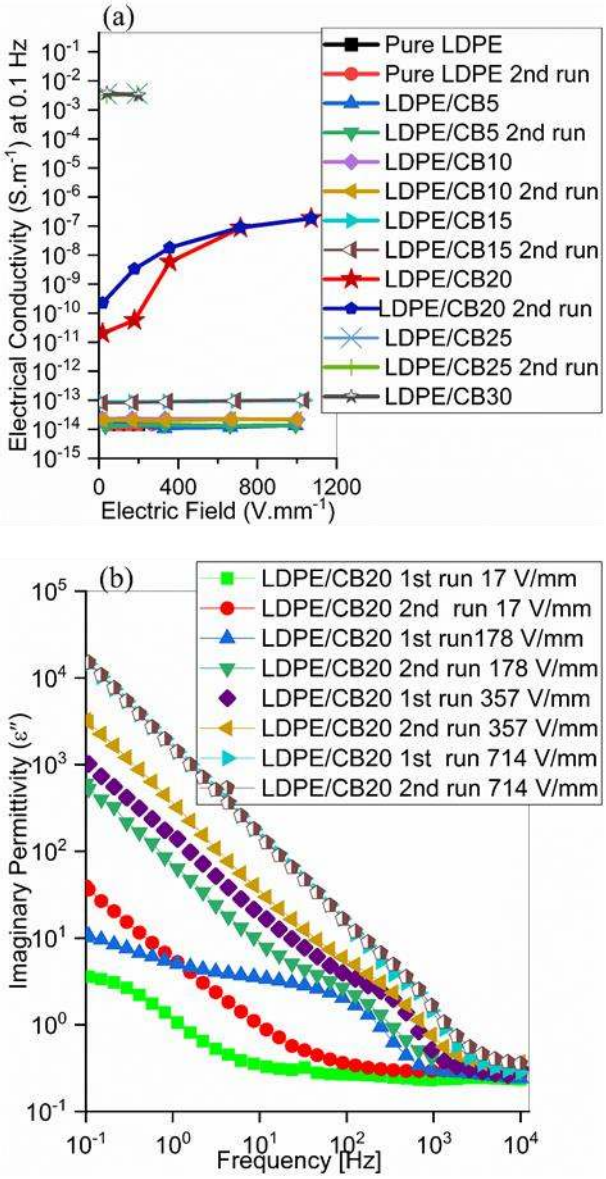

Figure 7. Real part of the complex conductivity at 0.1 Hz for several LDPE/CB composites as a function of the electrical field for the first two runs (a) and imaginary permittivity of the LDPE/CB20 composite at various electric fields (b).

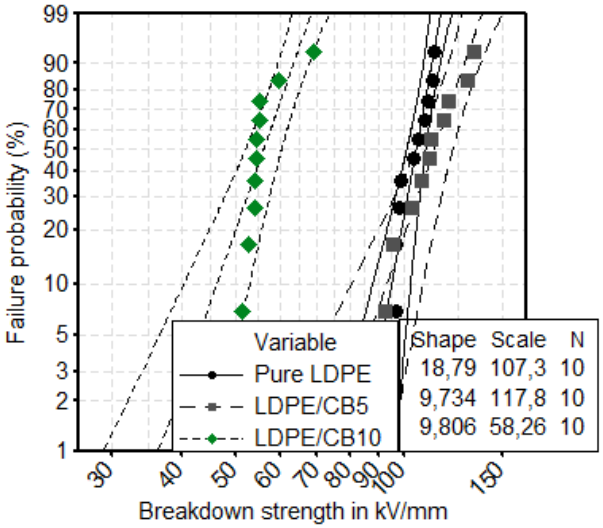

Figure 8. Weibull plots of the breakdown strengths with 95 % confidence intervals for the pure LDPE, LDPE/CB5 as well as LDPE/CB10 composite.

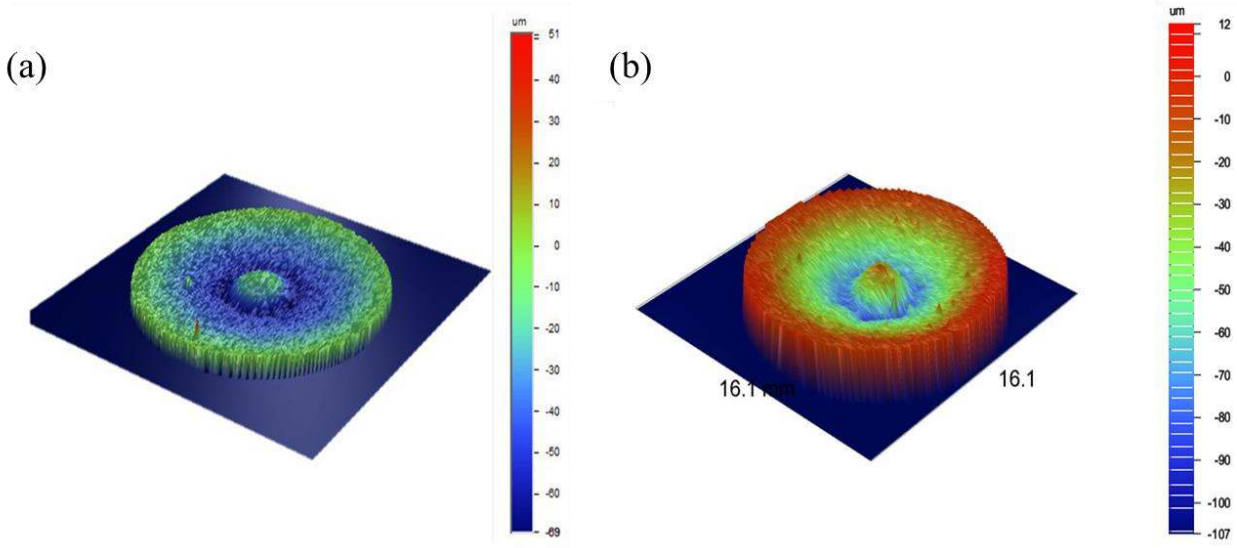

Figure 9. *Eroded areas of the samples subjected to corona condition: a) pure LDPE, b) LDPE/CB5 composite.*

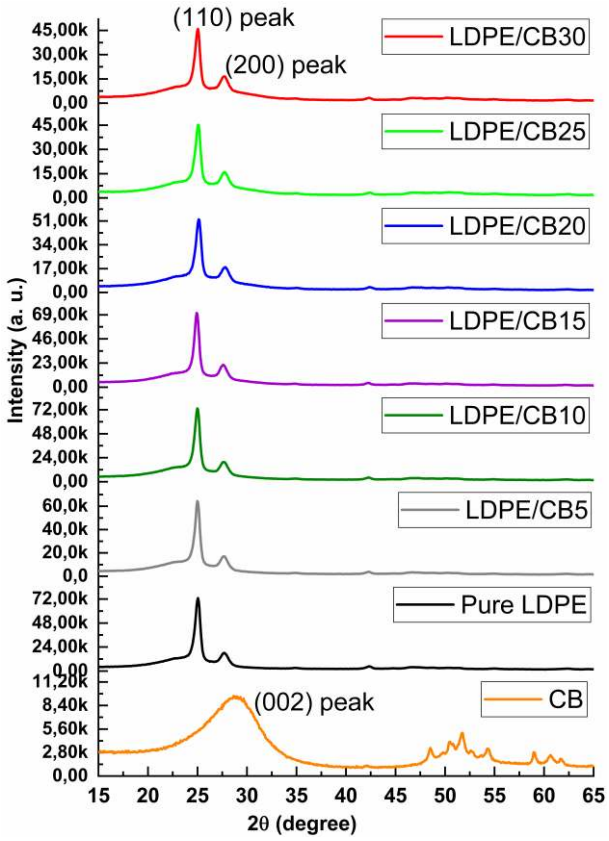

Figure 10. XRD patterns of CB, pure LDPE and its composites at different CB contents.

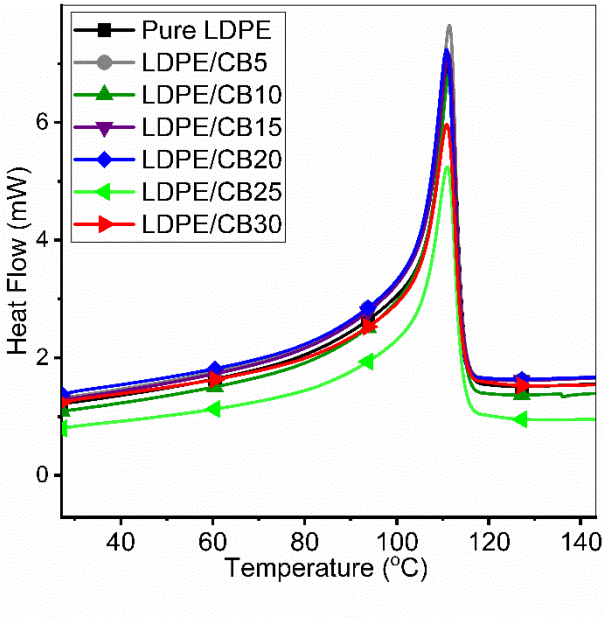

Figure 11. The heating thermograms of the pure LDPE and LDPE/CB composites, featuring the onset temperature and melting points.

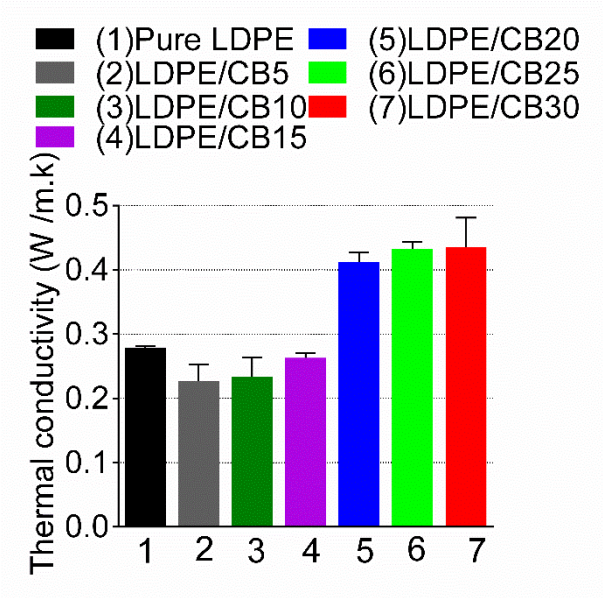

Figure 12. The thermal conductivity of LDPE/CB composites at different carbon black contents.

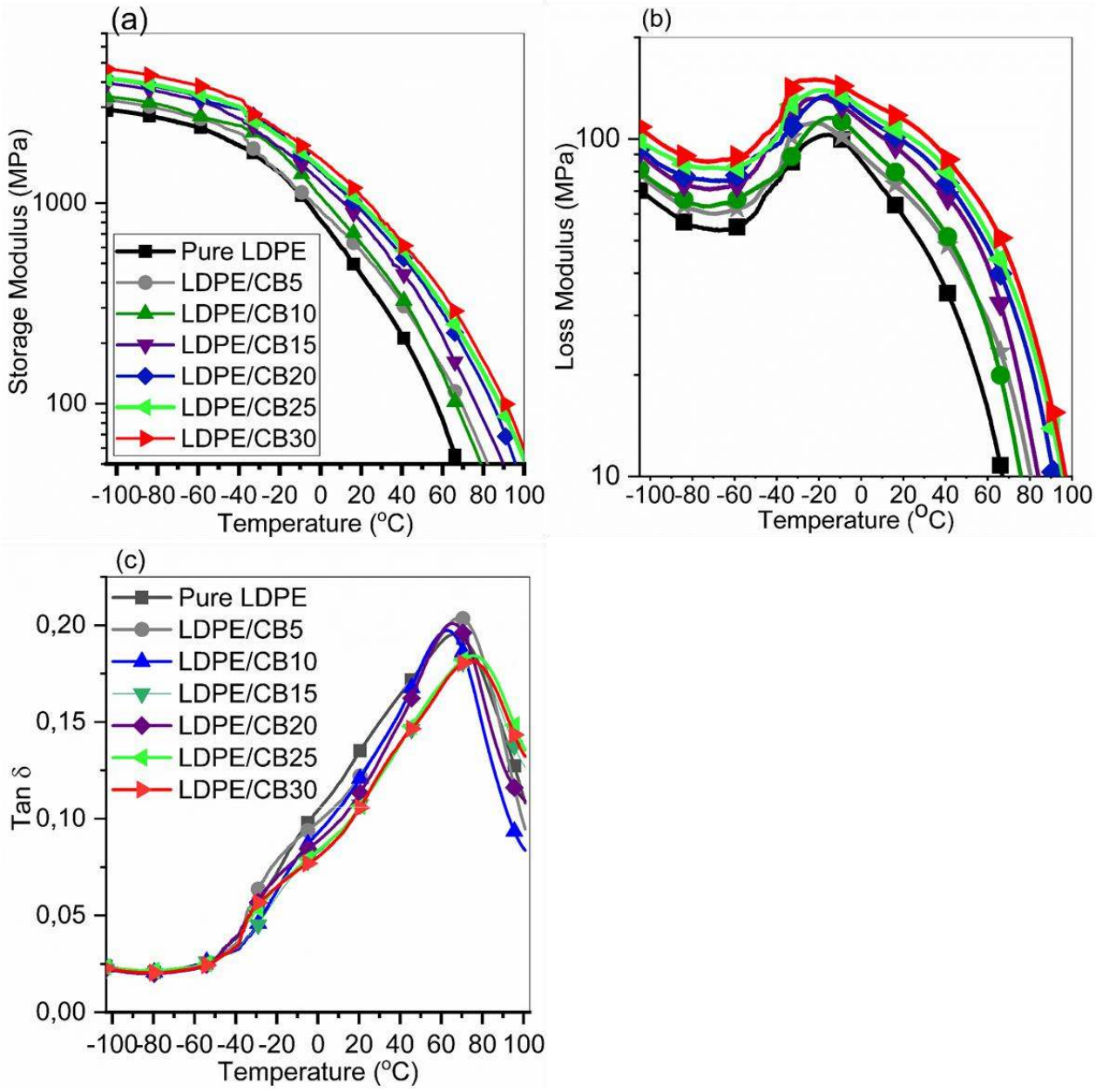

Figure 13. The log scale of the storage (a), loss (b) modulus and the tan δ (c) of LDPE/CB composites as a function of temperature (°C).

Table I. Formulations of the low-density polyethylene/carbon black composites prepared by melt compounding technique.

Sample	LDPE (wt %)	Carbon Black (wt %)
Pure LDPE	100	0
LDPE/CB5	95	5
LDPE/CB10	90	10
LDPE/CB15	85	15
LDPE/CB20	80	20
LDPE/CB25	75	25
LDPE/CB30	70	30

Table II. Comparison of electrical conductivity of various composites with different carbonaceous fillers.

Composites	Mixing procedure	Percolation threshold	Electrical conductivity ($S.m^{-1}$)	Reference
PA6/CNT	Melt blending	~ 2-3 wt%	10^{-5} at 2 wt%	[18]
PA6/TrGO	Melt blending	~ 5-10 wt%	10^{-5} at 10 wt%	[18]
TRG/PBT	Solvent-casting	0.22 vol%	10^{-2} at 0.4 vol%	[19]
TRG/PEE12	Solvent-casting	0.27 vol%	10^{-3} at 0.7 vol%	[19]
TRG/PEE30	Solvent-casting	0.31 vol%	10^{-3} at 0.7 vol%	[19]
TRG/PEE35	Solvent-casting	0.36 vol%	10^{-3} at 0.7 vol%	[19]
CPE/CB	Solvent-casting	10 wt%	10^{-2} at 10 wt%	[4]
LDPE/CNT	Roll mixing	-	10^{-9} at 2 wt%, 0.1 kV/mm	[13]
HDPE/CB	Grinding mill	0.1 vol%	10^{-1} at 0.11 vol%	[14]
LDPE/CB	Melt blending	2-7 wt%	10^{-7} at 7 wt%	[16]
PEDOT/ MWCNTs	Solvent-casting	-	293 S/m at 27 wt%	[17]
LDPE/CB	Melt compounding	20-25 wt%	10^{-1} at 25 wt%	Our work

*PA6 = Polycaprolactam, PEE = Polyester elastomer, PBT= Poly(butylene terephthalate), CPE = Chlorinated polyethylene, PEDOT= polyethylene dioxy thiophene.

Table III. Fitting parameters for dielectric response of LDPE/CB20 composite at 20 °C according to the Equation (5).

DC conductivity (S.cm^{-1})	Exponent N	$\Delta\varepsilon$ at 20 °C	τ (s)	α	β
8.50 x 10^{-14}	1.0	8.20	0.065	0.854	0.955

Table IV. The melting point, degree of crystallinity, lamellar thickness, onset temperature as well as the degradation temperature of the LDPE/CB composites measured by DSC and TGA.

	DSC results			TGA results		
Sample	T_m (°C)	X_c (%)	l (nm)	T at 5 wt% loss (°C)	T at 50 wt % (°C)	Residue (wt) % at 550 °C
Pure LDPE	111.61	41	7.62	376	464	0.26
LDPE/CB5	111.39	41	7.57	401	491	5.90
LDPE/CB10	111.30	40	7.55	404	479	9.11
LDPE/CB15	111.15	42	7.52	403	493	15.39
LDPE/CB20	110.80	43	7.44	401	498	20.16
LDPE/CB25	111.02	40	7.49	452	501	24.13
LDPE/CB30	110.85	40	7.45	409	492	29.37

Table V. Comparison of storage modulus of different carbonaceous-based composites with different matrices.

Composites	Mixing procedure	Storage modulus	Reference
PA6/TrGO	Melt blending	~ 3.6 GPa at 10 wt%	[18]
PA6/CNT	Melt blending	~ 2.8 GPa at 10 wt%	[18]
CPE/CB	Solvent-casting	~ 2.5 GPa at 10 wt% CB	[4]
LDPE/CB	Melt compounding	~ 4.2 GPa at 10 wt% CB	Our work